Reconfigurable memristor diode based on $CuInP_2S_6$/Graphene lateral heterojunction

Chuanzheng Liao,[1] Mengyao Zhang,[1] Yurong Jiang,[1, a)], Suicai Zhang,[1] Xueping Li,[1] Leiming Yu,[1] Xiaohui Song,[1] Kang Liu[2], Ding Wang[2] and Jianye Wang[2, a)], Congxin Xia[1, a)]

[1] Henan Key Laboratory of Advanced Semiconductor & Functional Device Integration, Henan Normal University, Xinxiang, 453007, China

[2] Institute of Physics, Henan Academy of Sciences, Zhengzhou 450046, China

[a)] Author to whom correspondence should be addressed: jiangyurong@whut.edu.cn, 121412584@qq.com, xiacongxin@htu.edu.cn

Characterizations and measurements:

The electronic properties were determined using a commercial Keysight B1500A. The Raman spectra and polarized Raman spectra were characterized using a Lab Ram HR800 with a 532 nm excitation laser. Atomic force microscopy (Bruker Multimode 8) was utilized to identify the thickness of the 2D materials. Kelvin probe force microscopy was utilized to acquire the contact potential difference (CPD) map of the 2D materials.

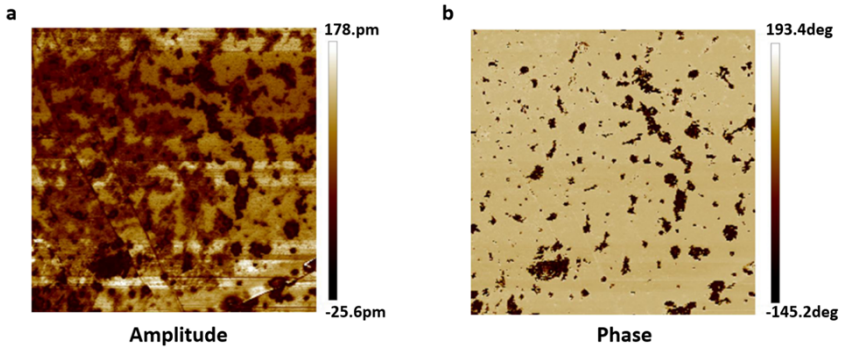

Fig. S1. (a) Vertical PFM phase. (b) Vertical PFM amplitude. These maps reveal the ferroelectric domains, and all of them clearly show ferroelectric domains.

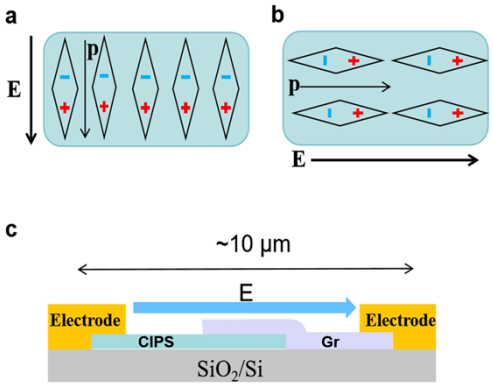

Fig. S2. (a) Polarization of ferroelectric materials under a vertical external electric field. (b) Polarization of ferroelectric materials under a horizontal electric field. (c) Schematic of the electric field (E) across the device, with typical device dimensions indicated.

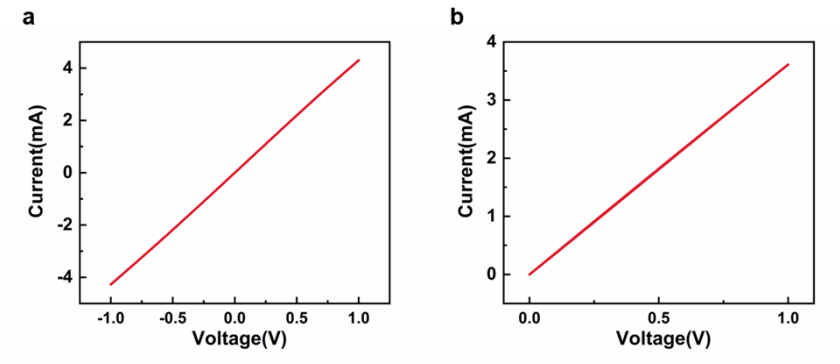

Fig. S3. (a) The *I-V* curve of graphene. (b) The *I*−*V* double sweep curves. It confirms that graphene forms a good ohmic contact with gold, and there is no hysteresis phenomenon.

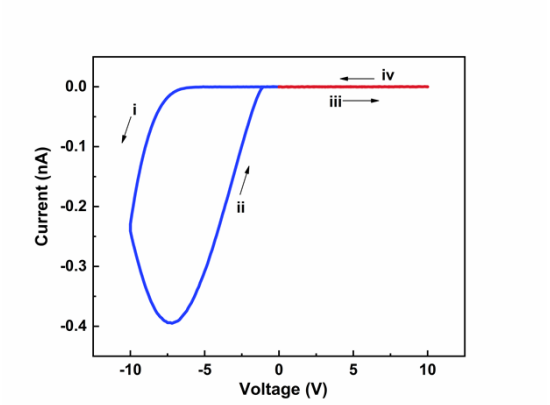

Fig. S4. The *I*−*V* double sweep curves of the device with a sweep direction from i → ii→ iii →iv. The graphs are asymmetric and exhibit a hysteresis phenomenon.

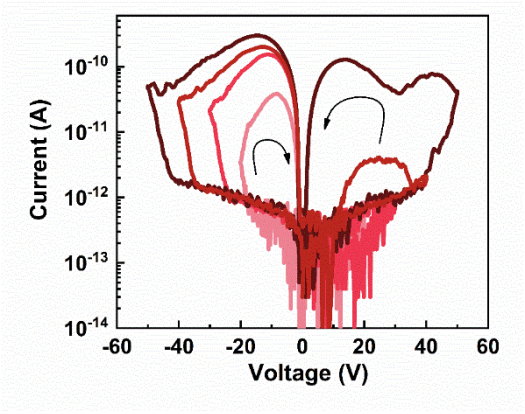

Fig. S5. The *I-V* curves of different sweep voltages and the hysteresis window gradually increase with the increase of the bias voltage sweep range. The direction of hysteresis is shown by the arrow in the figure.

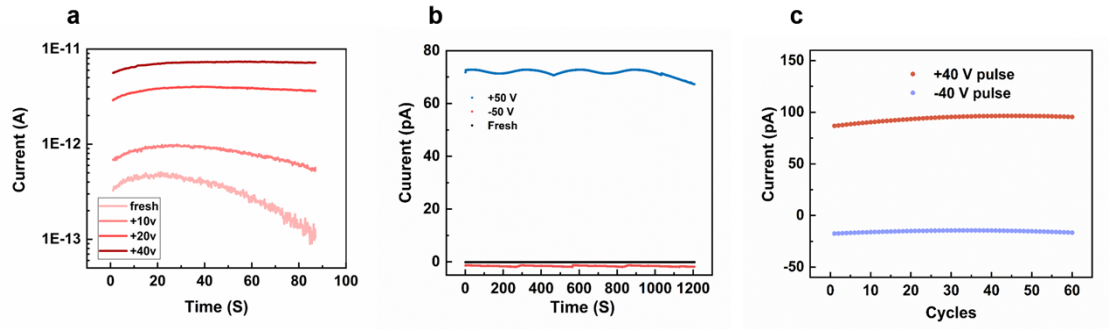

Fig. S6. (a) The *I-T* curves after applying different horizontal pulse amplitudes, with pulse voltages of +10 V, +20 V, +40 V, respectively. (b) The *I-T* curves for +50 V and -50 V pulses (pulse time is 20 s and read voltages are 1.5 V). The results show that the device has better modulation capability and a retention performance of more than 1000 s in air. (c) Switching of the device current measured at + 0.5 V during 60 polarization cycles, the pulse time of 6 s.

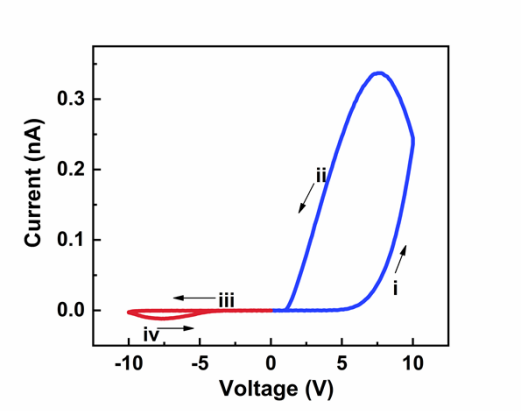

Fig. S7. The *I*−*V* double sweep curves of the device with direction i→ii→iii→iv. It has asymmetric graphs and hysteresis phenomenon and the opposite of the hysteresis window area in Fig. S4.

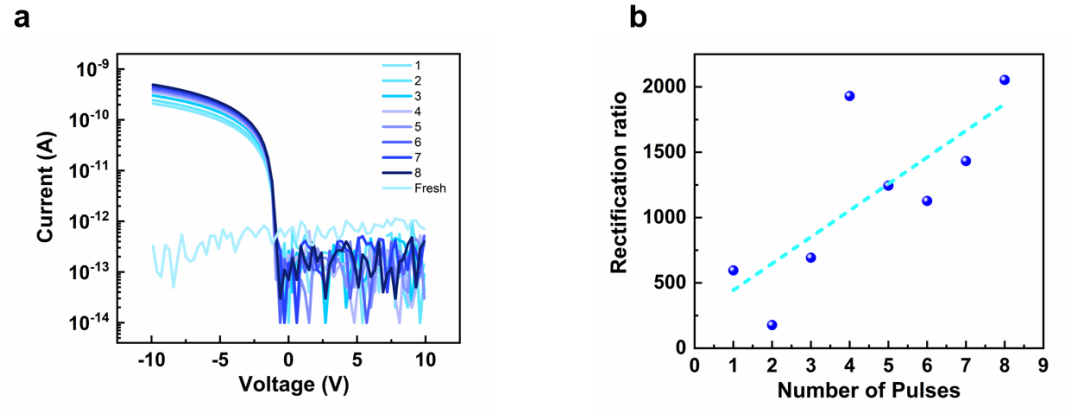

Fig. S8. (a) The *I*-*V* curves at different negative pulse times. (b) The relationship between the times of negative pulse and the rectification ratio shows excellent linear relationship.

Table S1. The three-line tables of the rectification ratio and switch ratio in the investigated literature.

Structure	The switching ratio	The rectification ratio	polling voltage	sweep voltage range	References
Au/Ti/In_2Se_3/Au/Ti	**500**	**10^3**	**4 V**	**0.3 V**	**49**
In/Au/In_2Se_3/In/Au	**~**	**300**	**5 V**	**2 V**	**50**
Ti//In_2Se_3/n-Si/InGa	**~**	**200**	**~**	**0.5 V**	**51**
Au/CulnP_2S_6/probe	**750**	**~10^3**	**5 V**	**5 V**	**30**
Au/CulnP_2S_6/Au	**~500**	**~10^2**	**50 V**	**50 V**	**31**
Bp/In_2Se_3	**~**	**~10^3**	**~**	**0.5 V**	**52**
Au/Pd/In_2Se_3/Au/Pd	**600**	**~10^3**	**~**	**4 V**	**53**
Ag/$CdPS_3$/ITO	**95**	**~**	**~**	**1 V**	**54**
Au/$HfSe_2$/Au	**100**	**~**	**1.5 V**	**1 V**	**55**
Au/CulnP_2S_6/Au	**700**	**~**	**15 V**	**10 V**	**56**
This work	**~10^3**	**>10^3**	**10 V**	**10 V**	

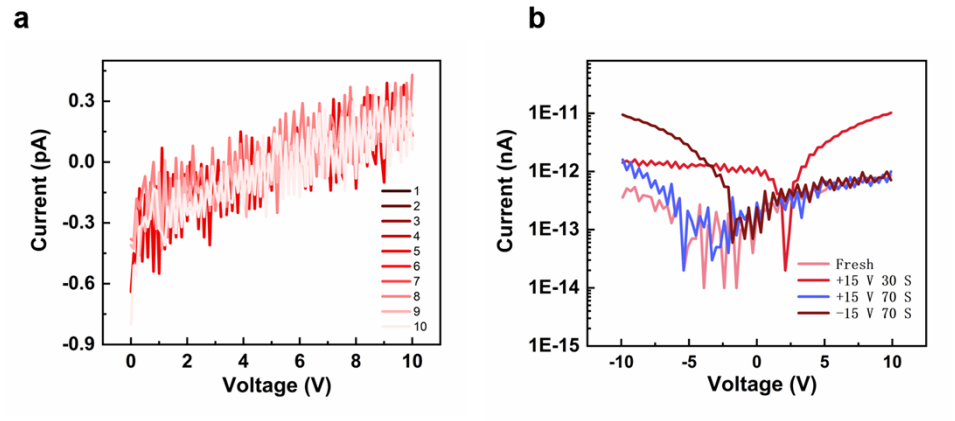

Fig. S9. (a) The *I-V* curves of Au / $CuInP_2S_6$ / Au device for multiple scans, Au is at the top. (b) The *I-V* curves after the initial state and different bias pulse. It can also be observed that controlling the conductivity of this structure is challenging, and the change in rectification characteristics are not pronounced.

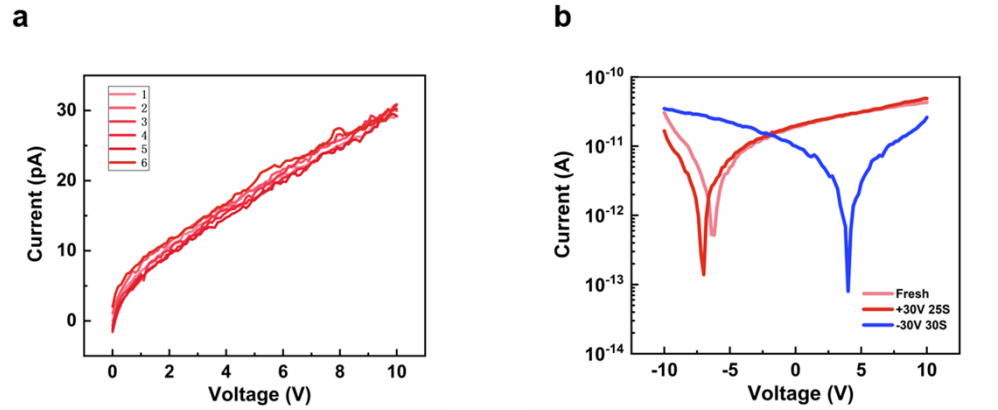

Fig. S10. (a) The *I-V* curves of Gr/ $CuInP_2S_6$ / Gr devices for multiple scans. (b) The *I-V* curves after the initial state and different bias pulse. It can also be observed that controlling the conductivity of this structure is challenging, and the change in rectification characteristics are not pronounced.

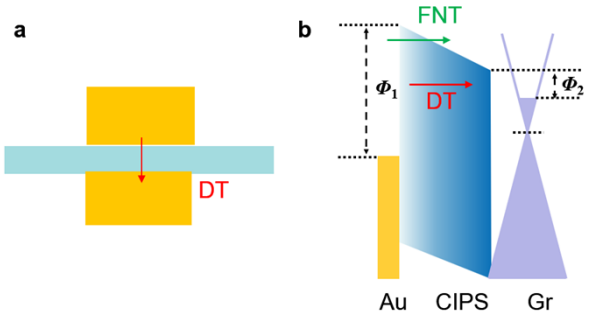

Fig. S11. (a) Diagram of the tunneling current perpendicular to the material. (b) Diagram of the tunneling current at heterojunction interface.

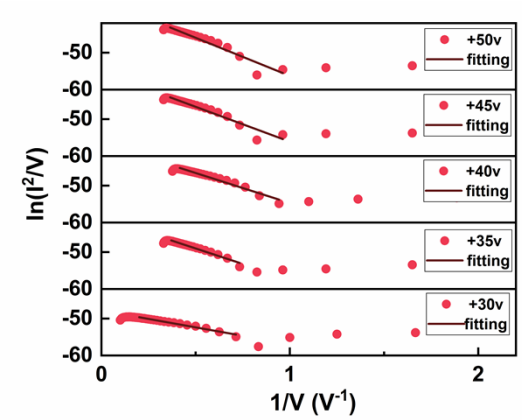

Fig. S12. Ln(I/V^2) vs $1/V$ plots, reconfigured from the I-V characteristics at different pulse amplitudes at room temperature, show the red dots as experimental data and the solid lines as fitted FN tunneling curves (the pulse voltage ranges from 30 V to 50 V in steps of 5 V). It can be observed that V_{trans} points shift to the right with the increase of pulse amplitude.

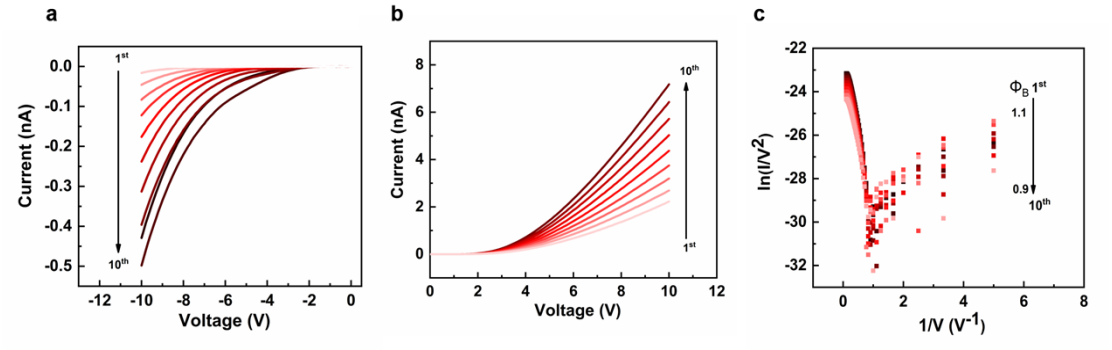

Fig. S13. (a) The $I-V$ curves measured with negative voltage sweeps. (b) The $I-V$ curves measured with positive voltage sweeps. (c) Ln(I/V^2) $-1/V$ Fowler-Nordheim tunneling plot for the positive voltage sweeps. With the increase in scanning times, the V_{trans} gradually decreases.

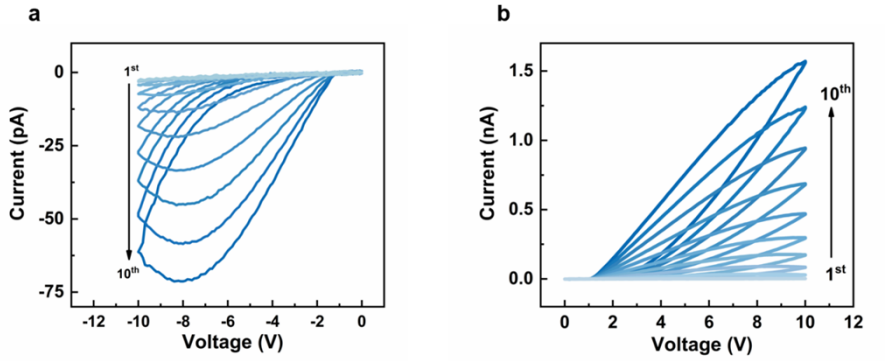

Fig. S14. (a) The $I-V$ double sweep curves measured with positive voltage sweeps. (b) The $I-V$ double sweep curves measured with negative voltage sweeps. As the number of scans increases, the current gradually increases, and the hysteresis window also widens.

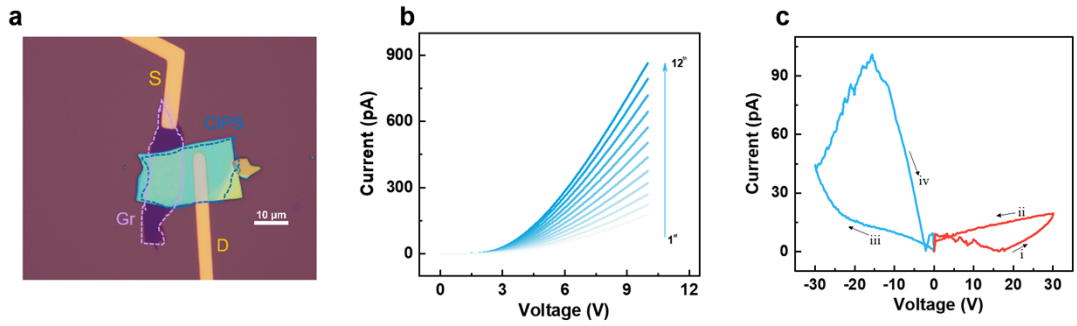

Fig. S15. (a) Optical image of the device; the purple and blue dashed regions represent Gr and CIPS, respectively; scale bar = 10 μm. (b) The *I-V* curves measured with positive voltage sweeps. (c) I-V double sweep curves of the device with a sweep direction from i→ii→iii→iv.

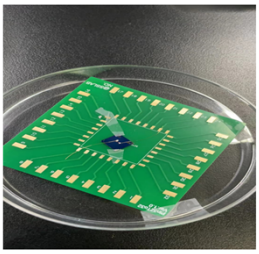

Fig. S16. Schematic diagram of the KPFM test setup. To begin, wire-bonding procedures were essential, using a gold wire bonder to affix the device to a specific Printed Circuit Board (PCB). This step is crucial for the subsequent application of lateral bias voltage pulses, enabling precise control and measurement in the experiment.